Chronophin coordinates cell leading edge dynamics by controlling active cofilin levels

Violaine Delorme-Walker[a,b], Ji-Yeon Seo[a,b], Antje Gohla[c], Bruce Fowler[a,b], Ben Bohl[a,b], and Céline DerMardirossian[a,b,1]

[a]Department of Immunology and Microbial Science, The Scripps Research Institute, La Jolla, CA 92037; [b]Department of Cell and Molecular Biology, The Scripps Research Institute, La Jolla, CA 92037; and [c]Department of Pharmacology, University of Würzburg, 97078 Wurzburg, Germany

Edited by Thomas D. Pollard, Yale University, New Haven, CT, and approved August 6, 2015 (received for review June 10, 2015)

Cofilin, a critical player of actin dynamics, is spatially and temporally regulated to control the direction and force of membrane extension required for cell locomotion. In carcinoma cells, although the signaling pathways regulating cofilin activity to control cell direction have been established, the molecular machinery required to generate the force of the protrusion remains unclear. We show that the cofilin phosphatase chronophin (CIN) spatiotemporally regulates cofilin activity at the cell edge to generate persistent membrane extension. We show that CIN translocates to the leading edge in a PI3-kinase–, Rac1-, and cofilin-dependent manner after EGF stimulation to activate cofilin, promotes actin free barbed end formation, accelerates actin turnover, and enhances membrane protrusion. In addition, we establish that CIN is crucial for the balance of protrusion/retraction events during cell migration. Thus, CIN coordinates the leading edge dynamics by controlling active cofilin levels to promote MTLn3 cell protrusion.

cofilin | chronophin | actin dynamics | cell protrusion | cancer cells

Cofilin is one crucial mediator of actin cytoskeletal dynamics during cell motility (1–5). At the cell edge, cofilin severs F-actin filaments, generating substrates for Arp2/3-mediated branching activity and contributing to F-actin depolymerization by creating a new pointed end and F-actin assembly by increasing the pool of polymerization-competent actin monomers (G-actin) (6, 7). Because of its ability to sever actin filaments and thus, modulate actin dynamics, the precise spatial and temporal regulation of cofilin activity at the cell leading edge is crucial to cell protrusion, chemotaxis, and motility both in vitro and in vivo (2, 8–13). Misregulation of cofilin activity and/or expression is directly related to diseases, including tumor metastasis (14–18) and Alzheimer's disease (19).

Several mechanisms regulate tightly the activation of cofilin in response to upstream stimuli, including interaction with phosphatidylinositol (4,5)-bisphosphate (20–22), local pH changes (23, 24), and phosphorylation at a single regulatory serine (Ser3) (8, 25). The phosphorylation of cofilin, leading to its inactivation, is catalyzed by two kinase families: the LIM-kinases [LIMKs(Lin11, Isl-1, and Mec-3 domain)] and the testicular kinases (25–27). Two primary families of ser/thr phosphatases dephosphorylate and reactivate the actin-depolymerizing and -severing functions of cofilin: slingshot (SSH) (28) and chronophin (CIN) (29).

SSH was identified as a cofilin phosphatase through genetic studies in *Drosophila* (28). The most active and abundant SSH isoform, SSH-1L, has been implicated in such biological processes as cell division, growth cone motility/morphology, neurite extension, and actin dynamics during membrane protrusion (30). SSH dephosphorylates a number of actin regulatory proteins in addition to cofilin, including LIMK1 (31) and Coronin 1B (32). CIN is a haloacid dehydrogenase-type phosphatase, a family of enzymes with activity in mammalian cells that has been poorly characterized. CIN dephosphorylates a very limited number of substrates (33) and as opposed to SSH, has little phosphatase activity toward LIMK both in vitro and in vivo; thus, it seems to be the more specific activator of cofilin (29, 30). CIN exhibits several predicted interaction motifs potentially linking it to regulation by PI3-kinase and phospholipase Cγ (PLCγ), both of which have been implicated in signaling to cofilin activation in vivo in MTLn3 adenocarcinoma cells (10, 34). CIN has been involved in cell division (29), cofilin–actin rod formation in neurons (35), and chemotaxing leukocytes (36, 37). The molecular mechanisms that control the activity and localization of CIN in cells are still not well-understood. In neutrophils, CIN mediates cofilin dephosphorylation downstream of Rac2 (36), and stimulation of protease-activated receptor2 results in recruitment of CIN and cofilin at the cell edge by β-arrestins to promote localized generation of free actin barbed ends, membrane protrusion, and chemotaxis (37). Chemotaxis to EGF by breast tumor cells is directly correlated with cancer cell invasion and metastasis (38, 39). Although cofilin activity is required for tumor cell migration, the contribution(s) of CIN to the regulation of actin dynamics at the leading edge has not yet been investigated.

The importance of cofilin in regulating tumor cell motility has been extensively studied using MTLn3 mammary carcinoma cells as a model system. The initial step of MTLn3 cell chemotaxis to EGF consists of a biphasic actin polymerization response resulting from two peaks of free actin barbed end formation (34, 40, 41). The first or early peak of actin polymerization occurs at 1 min after EGF stimulation and requires both cofilin and PLCγ activities (34), but it is not dependent on cofilin dephosphorylation (42). This first transient allows the cells to sense EGF gradients and initiate small-membrane protrusions (11). The second or late peak of actin polymerization occurs at 3 min and is dependent on both cofilin and PI3-kinase activities (43, 44). Cofilin activity in this late transient has been associated with full protrusion of lamellipodia (34). The mechanism by which cofilin becomes activated at the 3-min peak has not been identified, although it is likely to involve the phosphoregulation of Ser3 (42, 45).

Significance

Cell motility plays important roles in normal physiology and numerous disease states, including cancers. Cofilin, a key player in cell locomotion, controls the direction and the force of cell protrusion. Our study establishes the cofilin phosphatase chronophin (CIN) as a major component of a PI3-kinase–mediated, Rac1-dependent signaling mechanism that activates cofilin downstream of EGF receptor in mammary carcinoma cells. During EGF stimulation, CIN redistributes to the cell edge, where it regulates cofilin-dependent actin turnover and coordinates cell protrusion and retraction dynamics. Our data uncover previously unidentified molecular mechanisms regulating cofilin in time and space in tumor cells and expand our understanding of cancer cell movement, a critical step in the process of metastasis.

Author contributions: C.D. designed research; V.D.-W. and C.D. performed research; J.-Y.S., A.G., B.F., B.B., and C.D. contributed new reagents/analytic tools; V.D.-W. and C.D. analyzed data; and C.D. wrote the paper.

The authors declare no conflict of interest.

This article is a PNAS Direct Submission.

[1]To whom correspondence should be addressed. Email: dmceline@scripps.edu.

This article contains supporting information online at www.pnas.org/lookup/suppl/doi:10.1073/pnas.1510945112/-/DCSupplemental.

In this work, we determine the molecular mechanisms involved in the full protrusion of the leading edge upon EGF stimulation. We have identified CIN as a critical regulator of cofilin activation to coordinate leading edge dynamics. Our results yield insights into how CIN controls cell protrusion, a key step in the process of cell migration and metastasis.

Results

Spatial and Temporal Redistribution of CIN in EGF-Stimulated MTLn3 Cells. To determine whether the cofilin phosphatases CIN and/or SSH are involved in the formation of a second peak of barbed end, we first examined the subcellular distribution of CIN and SSH in MTLn3 cells at various times after EGF stimulation. Because there is no good CIN antibody for immunostaining, we overexpressed the protein in cells. It is important to note that cells are very sensitive to the expression level of CIN; they can become round and eventually, die. Therefore, a low amount of DNA was transfected into the cells for a short period (*Materials and Methods*), and only healthy cells (i.e., well-spread) were imaged in all of the immunofluorescence experiments. In resting cells, CIN WT (noted CIN) was diffusely distributed in the cytoplasm (Fig. 1*A*). Addition of EGF induced CIN recruitment to the leading edge beginning at 1 min and peaking by 3 min followed by a return to unstimulated levels by 5 min (Fig. 1*A*). Quantification of CIN fluorescence intensity to GFP intensity ratio from the leading edge toward the cell center indicated a 2.2-fold increase of CIN at the cell edge by 3 min compared with that of unstimulated cells (Fig. 1*B*, *Upper*). Moreover, this analysis indicated a widening of the region of CIN localization at 3 min compared with 1 min of stimulation. Interestingly, F-actin density at the cell edge correlated with CIN localization. Quantification of F-actin fluorescence intensity indicated an increase of F-actin at the leading edge at 1 min and peaking by 3 min followed by a return to 1-min levels by 5 min after EGF stimulation (Fig. 1*B*, *Lower*). It is interesting to note that the distribution of CIN in normal mammary epithelial cells or other breast cancer cells (SKBR3) (Fig. S1) upon EGF stimulation showed a similar pattern as in MTLn3 cells. Importantly, in contrast to CIN, analysis of SSH-1L subcellular distribution in MTLn3 cells revealed that SSH-1L^{WT} is largely cytoplasmic and does not translocate to the cell edge at any time after EGF stimulation (Fig. 1 *C* and *D*). In addition, quantification of F-actin fluorescent intensity showed no increase of F-actin at the cell edge on stimulation. This result can be explained by the fact that overexpression of SSH induces a global activation of cofilin in cells, which abolishes the cycle of local inactive/active cofilin at the cell edge that is required to induce the peaks of protrusion at 1 and 3 min. Together, our results indicate that the cofilin phosphatase CIN but not SSH-1L redistributes to the cell leading edge with a peak at 3 min after EGF stimulation.

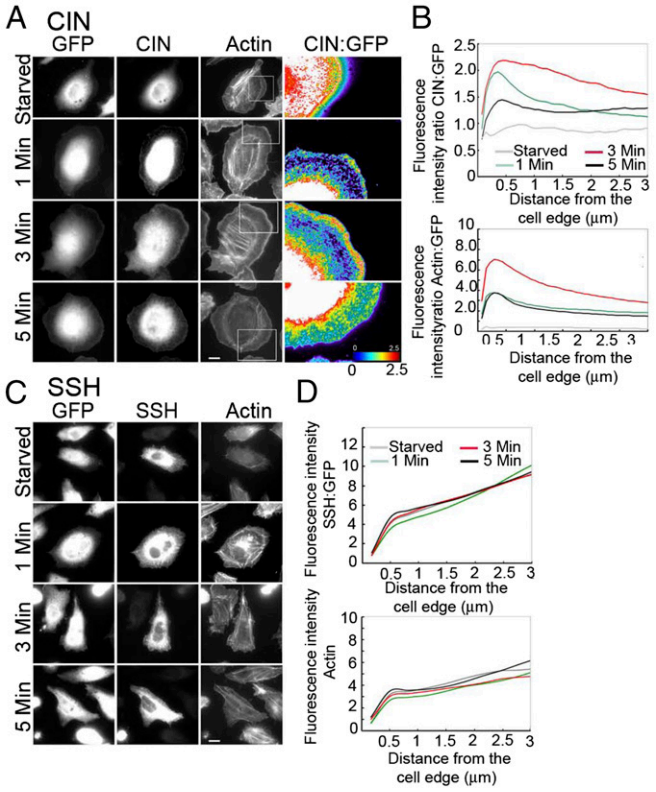

Fig. 1. Translocation of CIN at the leading edge of EGF-stimulated MTLn3 cells. (*A*) Localization of Myc-tagged CIN^{WT} and GFP control protein at 0, 1, 3, and 5 min after EGF stimulation. CIN to GFP ratio images are shown in column 4. Note an increase of CIN (red) at the cell leading edge at 3 min after EGF stimulation. (Scale bar: 5 μm.) (*B*) Fluorescence intensity ratios of Myc-tagged CIN^{WT}:GFP and Actin:GFP at the cell leading edge in starved conditions (gray) and at 1 (green), 3 (red), and 5 min (black) after EGF stimulation. (*C*) Localization of Myc-tagged SSH 1L^{WT} and GFP at 0, 1, 3, and 5 min after EGF stimulation. Note the absence of SSH translocation at the cell leading edge upon EGF stimulation. (Scale bar: 5 μm.) (*D*) Fluorescence intensity of SSH 1L and Actin at the cell edge in starved conditions (gray) and at 1 (green), 3 (red), and 5 (black) after EGF stimulation. The data shown represent one of three independent experiments and are averaged from $n \geq 25$ cells for each condition. The experiments were repeated three times with similar results.

CIN Activity Is Required for the Normal EGF-Stimulated Second Phase of Cofilin Activation. We next examined whether the recruitment of CIN to the cell edge during EGF stimulation coincided with cofilin activation [i.e., the disappearance of phosphocofilin (P-cofilin)]. In both control cells and cells expressing CIN^{WT}, P-cofilin was concentrated in the lamellipodium after 1 min of EGF stimulation (Fig. 2*A*). CIN^{WT} expression did not affect the amount of P-cofilin at the leading edge (quantification in Fig. 2*A*, *Right*). At 3 min, the P-cofilin level in the lamellipodium of control cells was decreased by ∼10% compared with that at 1 min of stimulation. Interestingly, there was a significant 26.3% ± 5.1% decrease in P-cofilin levels at 3 min in cells expressing CIN^{WT} compared with control cells (Fig. 2*B*).

To determine the contribution of endogenous CIN to the regulation of cofilin activity at the leading edge in response to EGF stimulation, we next examined the localization of inactive P-cofilin and total active cofilin in control and CIN-depleted cells. Depletion of CIN was first analyzed by Western blot using two differing rat CIN (rCIN) -targeting siRNA oligonucleotides (rCIN#1 and rCIN#4 like in *Materials and Methods*), both of which reduced cellular CIN levels by more than 80% compared with nontargeting (control) or human CIN-targeting siRNA oligonucleotides (Fig. S2 *A* and *B*). Normalized P-cofilin levels were higher by around 25% in CIN-depleted cells compared with siRNA control cells (Fig. S2*C*).

In starved control cells, both inactive P-cofilin and total cofilin diffusely distributed in the cytoplasm (Fig. 3*A*, *Upper*). Upon EGF stimulation, the P-cofilin levels at the cell leading edge were increased by 3.2- and 2-fold at 1 and 3 min, respectively, whereas the total cofilin levels increased by 2-fold at 1 and 3 min compared with starved cells (quantification in Fig. 3*A*). Quantification of the fluorescence intensity ratio of P-cofilin to cofilin at the cell leading edge revealed an increase of inactive P-cofilin at 1 min compared with starved cells and cells stimulated for 3 min with EGF (Fig. 3*A*, *Lower Right*). In starved CIN-depleted cells, P-cofilin and cofilin diffusely distributed in the cytoplasm as observed in control cells (Fig. 3*B*, *Upper*). At 1 min after EGF addition, we observed a narrow region of inactive P-cofilin and total cofilin at the cell edge that increased by 3.3- and 2-fold, respectively, compared with starved cells as indicated in the

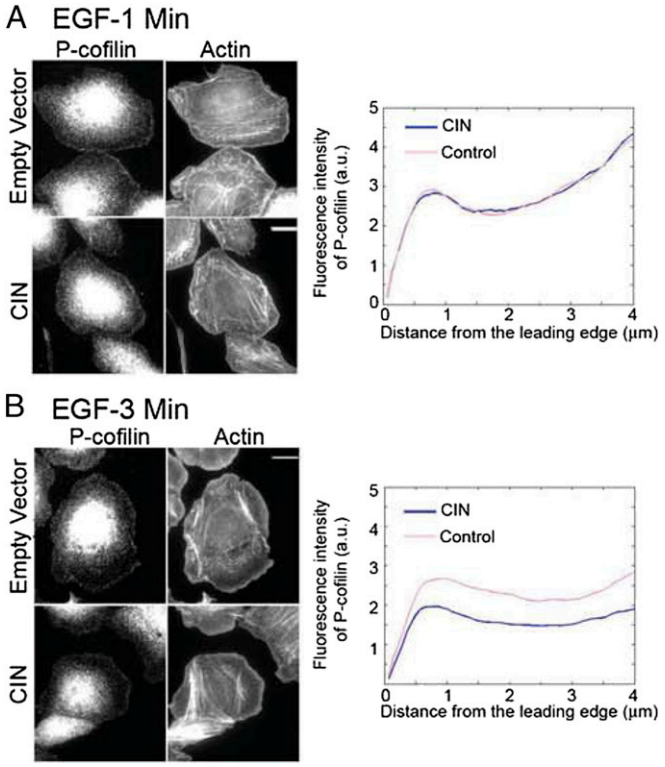

Fig. 2. CIN is active and regulates P-cofilin at the leading edge during EGF stimulation. P-cofilin and phalloidin staining in cells expressing empty vector or Myc-tagged CIN^{WT} at (*A*) 1 or (*B*) 3 min after stimulation with EGF. (Scale bar: 10 μm.) Quantification of fluorescent intensity of P-cofilin in control cells (pink) and cells expressing Myc-tagged CIN^{WT} (blue) at 1 and 3 min after EGF stimulation is shown in *Right*. Representative profiles of three independent experiments are shown, in which an average of 45 cells per experiment was analyzed.

quantification analysis (Fig. 3*B*, *Lower Left* and *Lower Center*). These protein levels were very similar to those obtained in control siRNA cells (Fig. 3*A*). Interestingly, in CIN-depleted cells after 3 min of EGF addition, we observed a wide region of P-cofilin at the cell leading edge (Fig. 3*B*). Quantification of fluorescence intensity revealed an ~5-fold increase of inactive P-cofilin compared with starved cells, whereas cofilin levels increased by only 1.5-fold. The fluorescence intensity ratio of P-cofilin to cofilin was similar in control and CIN-depleted cells in starved conditions and at 1 min upon EGF addition (compare quantifications in Fig. 3 *A*, *Lower Right*, red and green lines and *B*, *Lower Right*, red and green lines). In contrast, after 3 min of EGF stimulation, the ratio of P-cofilin to cofilin levels increased dramatically in CIN-depleted cells compared with control cells (compare quantifications in Fig. 3 *A*, *Lower Right*, black line and *B*, *Lower Right*, black line). These data suggest that CIN does not affect cofilin phosphorylation at 1 min after EGF stimulation but that CIN is important to cofilin activation at 3 min after EGF addition.

Together, these results indicate that CIN is active at the leading edge and that its activity is required for the EGF-stimulated second phase of cofilin activation within the lamellipodium.

CIN Localization at the Leading Edge of MTLn3 Cells at 3 Min Is Dependent on a PI3-Kinase and Rac1 Pathway. Previous studies have shown that PI3-kinase selectively regulates the 3-min actin filament free barbed end transient observed in EGF-stimulated MTLn3 cells (34). We examined whether PI3-kinase activity might be necessary for EGF-stimulated CIN accumulation at the cell edge. We observed that wortmannin treatment effectively inhibited CIN recruitment to the leading edge at 3 min after EGF addition compared with DMSO control (Fig. 4*A*). This result indicates that PI3-kinase activity is important for CIN recruitment to the cell leading edge in response to EGF stimulation.

To determine whether this effect was caused by a direct regulation of PI3-kinase activity on CIN localization, we examined the effects of perturbing the signaling components downstream of PI3-kinase. Because it is known that PI3-kinase activity often induces the activation of Rac1 GTPase (46, 47), we, therefore, transfected MTLn3 cells with CIN^{WT} and either constitutively active Rac1 (GFP-tagged Rac1 Q61L) or GFP empty vector control. As shown in Fig. 4*B*, expression of constitutively active Rac1 rescued the inhibition of EGF-induced CIN translocation to the leading edge caused by the PI3-kinase inhibitor (compare

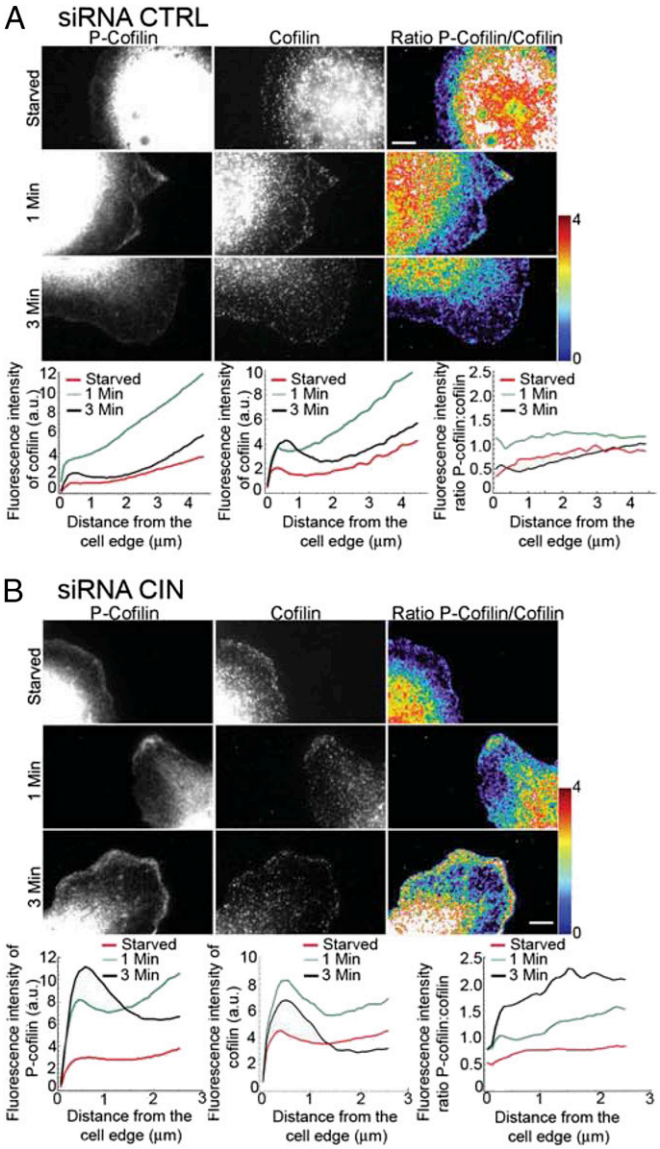

Fig. 3. Increase of the P-cofilin level in CIN-depleted MTLn3 cells at 3 min after EGF stimulation. P-cofilin and cofilin staining in (*A*) control siRNA (siRNA CTRL) cells or (*B*) CIN siRNA-transfected cells at 0, 1, and 3 min after EGF stimulation. Column 3 in *A*, *Upper* and *B*, *Upper* shows the ratio of P-cofilin to cofilin levels. Fluorescence intensities were analyzed with Matlab, and representative profiles from four independent experiments are shown in *A*, *Lower* and *B*, *Lower* (blue, 3 min of EGF; green, 1 min of EGF; red, starved). An average of 48 cells per experiment was analyzed for quantification. (Scale bar: 5 μm.)

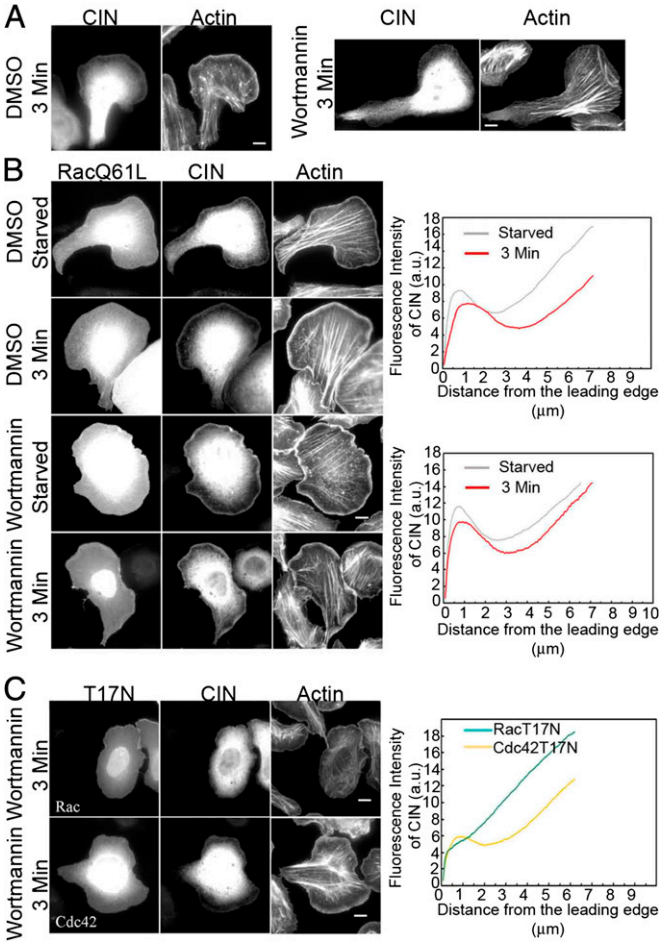

Fig. 4. CIN localization at the leading edge is dependent on a PI3-kinase–Rac1 pathway. (*A*) Myc-CIN^{WT} and phalloidin staining in cells treated with DMSO or 100 nM wortmannin before EGF stimulation for 3 min. (*B*, *Left*) Myc-CIN^{WT} and phalloidin staining in cells expressing constitutively active Rac1 (GFP-Rac Q61L) treated with either (rows 1 and 2) DMSO or (rows 3 and 4) wortmannin at 0 and 3 min after EGF stimulation. (Scale bar: 5 μm.) *B, Right* shows the fluorescence intensity of Myc-tagged CIN^{WT} in cells expressing Rac1 Q61L treated with DMSO or wortmannin measured from the cell edge (0 μm) into the cell center (10 μm; gray, starved; red, 3 min of EGF). The data shown represent one experiment and are averaged from $n \geq 21$ cells for each condition. The experiment was repeated three times with similar results. (*C*) Myc-CIN^{WT} and phalloidin staining in cells expressing dominant-negative constructs (*Upper Left*) GFP-Rac1 T17N or (*Lower Left*) GFP-Cdc42 T17N and treated with wortmannin on a 3-min EGF stimulation. (Scale bar: 5 μm.) *Right* shows the fluorescence intensity of Myc-tagged CIN^{WT} in cells expressing Rac1 T17N (green) or Cdc42 T17N (yellow) measured from the cell edge (0 μm) into the cell center (10 μm). The data shown represent one experiment and are averaged from $n \geq 10$ cells for each condition. The experiment was repeated three times with similar results.

the wortmannin conditions in Fig. 4 *A* and *B*). Interestingly, although CIN redistributed to the cell membrane only after EGF stimulation in control cells, we observed an accumulation of CIN at the cell leading edge even in starved conditions in cells expressing Rac1 Q61L [compare the starved conditions (DMSO or wortmannin) in Figs. 1*A* and 4*B*]. Quantification of CIN fluorescence intensity at the cell leading edge in starved or EGF-stimulated conditions in cells treated with DMSO or wortmannin revealed a similar amount of CIN accumulation (Fig. 4*B*, *Right*). These results indicate that constitutively active Rac1 is sufficient for the translocation of CIN to the cell edge and that Rac1 acts downstream of PI3-kinase to regulate CIN recruitment in response to EGF stimulation.

Because Cdc42 activation at the leading edge of MTLn3 cells stimulated with EGF has been reported to be biphasic, with peaks of activation at 50 s and 3 min (48), we tested whether activation of Cdc42 could be involved in the relocalization of CIN at 3 min. To this end, MTLn3 cells were cotransfected with CIN^{WT} and constitutively active Cdc42 (GFP-Cdc42 Q61L) in the presence of DMSO or wortmannin. In DMSO-starved conditions, CIN was mainly localized in the cytoplasm. Upon EGF stimulation, we observed an accumulation of CIN at the cell leading edge at 3 min (Fig. S3*A*, rows 1 and 2). Interestingly, active Cdc42 did not rescue the inhibition of EGF-induced CIN translocation to the leading edge caused by wortmannin (Fig. S3 *A*, rows 3 and 4 and *B*). Finally, cells were transiently transfected with either dominant-negative GFP-tagged Rac1 T17N or Cdc42 T17N. In control, GFP alone did not affect CIN translocation (Fig. 1*A*). Dominant-negative Rac1 but not Cdc42 effectively suppressed the recruitment of CIN to the cell edge at 3 min post-EGF stimulation (quantification in Fig. 4*C*). Taken together, these results indicate that the EGF-stimulated, PI3-kinase–mediated effect on CIN distribution in cells is likely caused by downstream activation of an Rac1-dependent pathway.

β-Arrestins Are Not Required for CIN Localization at the Cell Edge in MTLn3 Cells. β-Arrestins have been shown to scaffold cofilin and CIN in primary leukocytes and MDA-MB 468 breast cancer cells. This complex formation at the lamellipodia is required to induce membrane protrusion in MEF (mouse embryonic fibroblast) cells (37). To decipher the molecular mechanisms that regulate the translocation of CIN at the MTLn3 cell edge after EGF stimulation, we tested whether arrestin proteins were required. To test this hypothesis, we depleted both rat β-arrestin 1 (ARB1) and ARB2 protein levels using RNAi (49) and analyzed the distribution of CIN in cells upon EGF stimulation. Because the commercial antibodies for both arrestin proteins are not good for Western blot or immunostaining, we first analyzed the efficiency of arrestin depletion in cells by immunofluorescence using paxillin antibody. Indeed, the number of focal adhesions has been shown to increase in cells lacking β-arrestins compared with control cells (50). We found that depletion of β-arrestins (ARB1, ARB2, or both) led to an enhanced formation of focal adhesions compared with control cells, thus indicating reduced cellular β-arrestin levels (Fig. S4*A*). We next cotransfected β-arrestin–targeting siRNA oligos with Myc-CIN and compared the distribution of CIN with nontargeting siRNA oligo control cells upon EGF stimulation. Similar to control cells (Fig. S4*B*), we observed that siRNA-mediated knockdown of ARB1, ARB2, or both resulted in CIN recruitment to the cell leading edge beginning at 1 min and peaking by 3 min followed by a decrease by 5 min (quantification in Fig. S4 *C*, *Right*, *D*, *Right*, and *E*, *Right*). Quantification of CIN fluorescence intensity to GFP intensity ratio from the leading edge toward the cell center in β-arrestin–depleted cells indicated a similar increase of CIN at the cell edge by 3 min compared with that in control cells (Fig. S4 *B*, *Right*, *C*, *Right*, *D*, *Right*, and *E*, *Right*). These data indicate that ARBs are not required for CIN localization at the cell edge upon EGF stimulation.

CIN Localization at the Cell Edge Is Not Dependent on F-Actin Accumulation. Redistribution of CIN at the cell leading edge correlated with F-actin accumulation, suggesting a possible binding of CIN with F-actin. To test this hypothesis, we examined whether CIN interacts directly with F-actin by using high-speed actin cosedimentation assays. Recombinant His-CIN was exclusively detected in the soluble fraction in the presence or absence of F-actin (Fig. 5 *A*, Western blot and *C*, quantification). In control, the amount of the F-actin binding protein α-actinin localized in the pellet fraction was 90.9% ± 2.0% in the presence of F-actin and 29.1% ± 8.7% in the absence of F-actin as determined by Coomassie Blue-stained gels. The nonactin binding protein, BSA (bovine serum albumin),

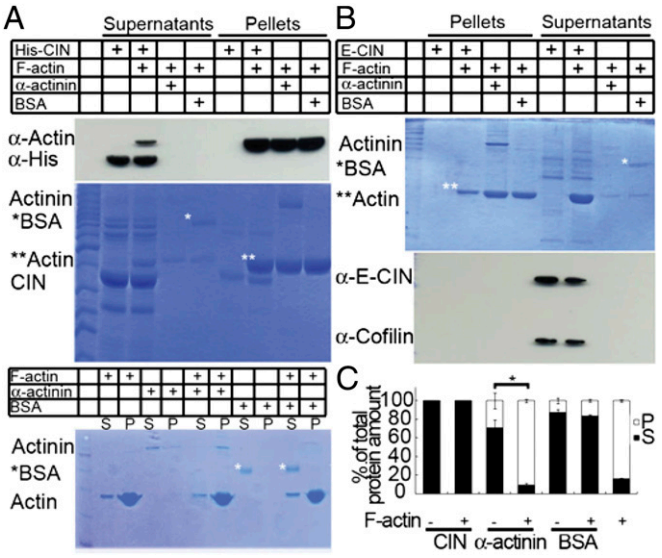

Fig. 5. CIN does not bind F-actin as determined by F-actin sedimentation assay. (*A*, *Top*) Representative immunoblot showing an absence of F-actin binding to recombinant purified His-CIN in the pellets of high-speed cosedimentation experiments. (*A*, *Middle*) Representative Coomassie Blue-stained gel showing the corresponding supernatants and pellets. (*A*, *Bottom*) Representative Coomassie Blue-stained gel showing the binding of α-actinin to F-actin as a positive control and the absence of binding of BSA to F-actin as a negative control. (*B*, *Upper*) Representative Coomassie Blue-stained gel showing the nonbinding of F-actin to purified GFP-CIN. Note the presence of a high amount of solubilized actin in the supernatant. *B*, *Lower* represents an immunoblot showing the binding of purified GFP-CIN to endogenous cofilin (E-cofilin). (*C*) Quantification of the total amount of proteins in the pellet (P; white) or supernatant (S; black) in the presence or absence of F-actin. Mean ± SEM. $*P < 0.05$.

was found in the supernatant in presence or absence of F-actin at 87.5% ± 3.2% and 83.8% ± 1.6%, respectively (Fig. 5 *A*, *Middle* and *Bottom* and *C*, quantification). We next performed the F-actin cosedimentation assays with GFP-CIN expressed and purified from HeLa cells. Similar to the previous experiments, F-actin was located in the pellet (Fig. 5*B*, Coomassie Blue-stained gel), whereas purified GFP-CIN was only observed in the supernatant (Fig. 5 *B*, *Lower* and *C*). Together, these data show that CIN does not bind F-actin.

Cofilin Regulates CIN Translocation at the Cell Edge. Interestingly, the Coomassie Blue-stained gels revealed an important amount of solubilized actin in the supernatant under conditions where F-actin was incubated with purified GFP-CIN (Fig. 5*B*, Coomassie Blue gel). These data might indicate a severing of F-actin. Because cofilin binds to and severs F-actin and is a substrate for CIN, we tested the hypothesis that CIN could interact with endogenous cofilin. Purified GFP-CIN was blotted against cofilin antibody (Fig. 5*B*, *Lower*). The data revealed an interaction between GFP-CIN and cofilin. Because cofilin localizes at the cell leading edge and we found that it binds to CIN, we tested whether cofilin could contribute to CIN redistribution to the lamellipodia upon EGF stimulation. To this end, we compared CIN distribution in cells depleted in cofilin with control cells using a shRNA (Fig. 6*A*). Plasmids expressing a control shRNA or shRNA against rat cofilin were transfected into MTLn3 cells overexpressing Myc-CIN. Interestingly, in contrast to control shRNA cells, depletion of cofilin impaired the localization of CIN at the cell edge in response to EGF (quantification in Fig. 6 *B*, *Center*, *C*, *Center*, and *D*, *Center*). Of note, F-actin still accumulated in the lamellipodium of cofilin-depleted cells (quantification in Fig. 6 *B*, *Right*, *C*, *Right*, and *D*, *Right*), confirming our previous results in vitro on the lack of CIN binding to F-actin. Altogether, these results indicate that cofilin is required for the cell leading edge localization of CIN during EGF stimulation.

CIN Increases EGF-Induced Generation of Free Actin Barbed Filament Ends. In MTLn3 carcinoma cells, EGF-induced cofilin activation and actin polymerization are directly correlated with the generation of free actin barbed filament ends, with peaks at 1 and 3 min after stimulation (34). We examined whether CIN expression and translocation affected cofilin-dependent free barbed end formation during EGF stimulation. As shown in Fig. 7*A*, after addition of EGF for 1 min, control cells and cells expressing CIN^{WT} exhibited a comparable level of actin free barbed ends localized in a narrow rim along the leading edge. Conversely, after 3 min of stimulation with EGF, CIN^{WT} increased the generation of free barbed ends at the cell periphery within the major protrusion, enhancing both the width and intensity of the rim of barbed end staining compared with cells expressing empty vector control under the same conditions (Fig. 7*B*). Quantitative analysis of free barbed

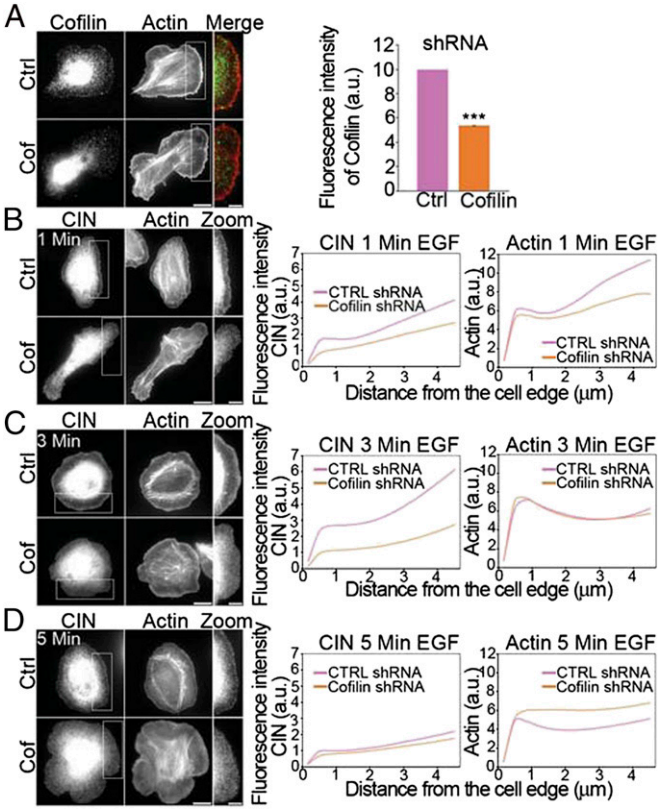

Fig. 6. Cofilin is required for the translocation of CIN at the cell leading edge. (*A*, *Left*) Depletion of cofilin in MTLn3 cells. MTLn3 cells were transfected with shRNA constructs, stimulated with EGF, and stained for endogenous cofilin (green in merge) and F-actin (red in merge). (Scale bar: 10 μm.) Column 3 shows zoomed regions of the white boxes shown in the actin column. (Scale bar: 5 μm.) Quantification of the fluorescence intensity of cofilin is shown in *A*, *Right*. Mean ± SEM. $***P < 0.001$. (*B–D*) Effect of cofilin depletion on CIN translocation. MTLn3 cells were transfected for 36 h with cofilin-targeting or control shRNA constructs. Cells were then transfected with shRNA constructs combined with Myc-tagged CIN^{WT} and stimulated with EGF for (*B*) 1, (*C*) 3, or (*D*) 5 min. Cells were fixed and stained with anti-Myc antibodies (CIN) and phalloidin (Actin). (Scale bar: 10 μm.) Zoomed regions of the white boxes in the CIN column are shown in column 3 in *B*, *Left*, *C*, *Left*, and *D*, *Left*. (Scale bar: 5 μm.) Graphs in *Center* and *Right* represent the quantification of the fluorescence intensity of CIN and actin as a function of the distance from the leading edge. Each graph is an average of 18–29 cells per condition. Note the absence of CIN recruitment at the cell leading edge in cells depleted in cofilin (orange) compared with control cells (pink). Cof, cofilin; Ctrl, control.

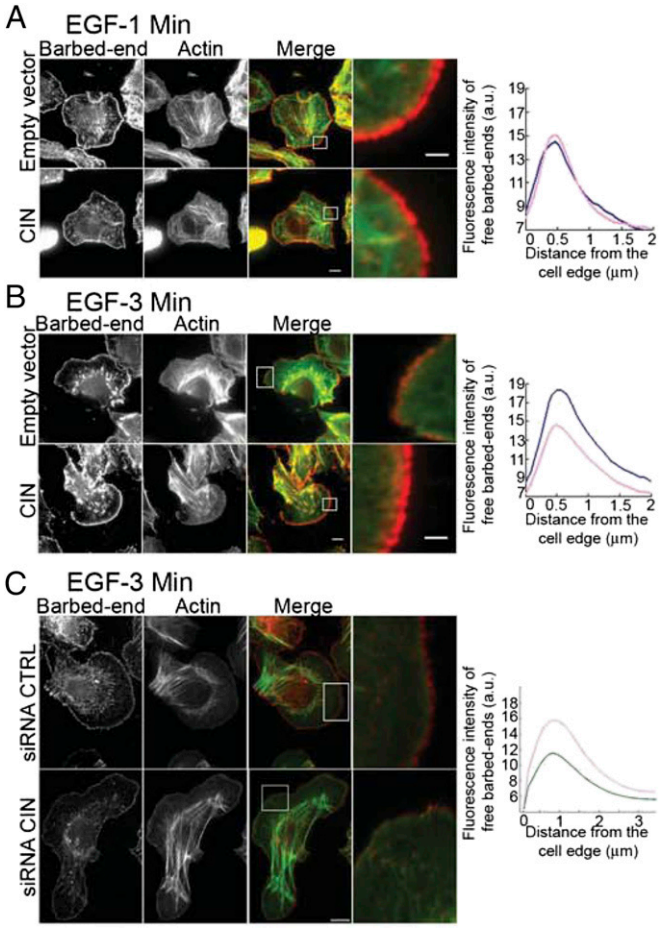

Fig. 7. CIN regulates the formation of free actin filament barbed ends after EGF stimulation. Free barbed end actin incorporation (red) and F-actin phalloidin (green) staining at (*A*) 1 and (*B*) 3 min after stimulation with EGF in cells expressing empty vector or Myc-tagged CIN^{WT}. (Scale bar: 5 μm.) Boxed regions are shown in higher magnification in column 4 in *A*, *Left* and *B*, *Left*. (Scale bar: 5 μm.) Fluorescence intensity of free barbed ends in control (pink) and Myc-tagged CIN^{WT} (blue) measured from the cell edge (0 μm) into the cell center (2 μm). Representative profiles of three separate experiments are shown, in which an average of 36 cells was analyzed for each experiment. (*C*) Free barbed end actin incorporation (red) and F-actin phalloidin staining (green) at 3 min after stimulation with EGF in (*Upper Left*) control siRNA (CTRL) or (*Lower Left*) CIN siRNA. (Scale bar: 5 μm.) Boxed regions are shown in higher magnification in column 4 in *Left*. (Scale bar: 5 μm.) *Right* shows the fluorescence intensity of free barbed end formation. A representative profile of three independent experiments is shown. An average of 40 cells per experiment was analyzed.

end fluorescence intensity (Fig. 7*B*, *Right*) confirmed our observations, showing an ~50% increase in free barbed ends at the periphery of cells expressing CIN^{WT} 3 min after EGF stimulation. These data are in line with the study by Kiuchi et al. (6) showing that active cofilin contributes to stimulus-induced actin filament assembly by supplying an abundant pool of actin monomers in cytoplasm.

To determine whether depletion of endogenous CIN protein affected EGF-induced free barbed end formation at the cell edge, we treated MTLn3 cells with low concentrations of rCIN-specific siRNA oligonucleotides (rCIN#1 or rCIN#4). CIN depletion in MTLn3 cells had no effect on the formation of free actin barbed ends detected at 1 min but significantly decreased by 30% ± 8.2% the generation of free actin barbed ends at the cell leading edge at 3 min after EGF addition compared with siRNA controls (Fig. 7*C*). Together, these results indicate that CIN becomes active at the leading edge at 3 min upon EGF stimulation, coincident with its EGF-induced translocation, and that CIN activity is required for the second phase of EGF-stimulated free barbed end formation within the lamellipodium.

Effect of CIN on Actin Dynamics at the Leading Edge. To examine the effects of CIN on actin dynamics at the leading edge in greater quantitative detail, we monitored by spinning disk confocal fluorescent speckle microscopy (FSM) MTLn3 cells injected with a low level of rhodamine-conjugated actin (Movies S1–S4). The speckled appearance of fluorescent actin in these cells allowed us to measure F-actin retrograde flow by kymograph analysis and analyze the distribution of the lamellipodium and the lamella actin networks at the leading edge. In control cells (Movie S1), F-actin underwent a fast retrograde flow (1.436 ± 0.078 μm/min) in the lamellipodium and a slow retrograde flow (0.441 ± 0.029 μm/min) in the lamella (Fig. 8 *A* and *C*). Expression of CIN^{WT} (Movie S2) did not significantly alter the flow velocity in the lamellipodium (1.426 ± 0.119 μm/min; $P = 0.94$ compared with control cells) but increased the rate of F-actin retrograde flow further inside the protrusion (0.825 ± 0.078 μm/min) (Fig. 8 *A*–*C*). Indeed, these cells exhibited only a single distinct region of fast F-actin retrograde flow at the cell edge (Fig. 8*A*).

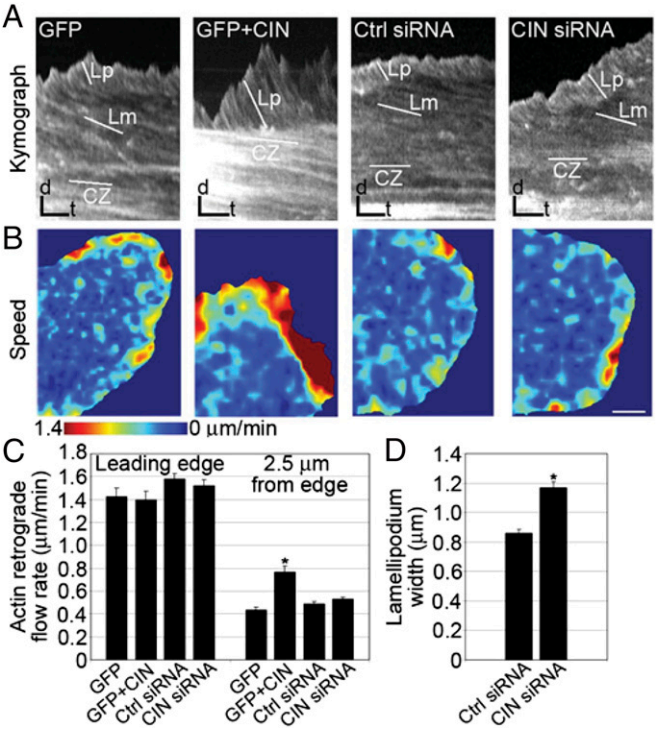

Fig. 8. CIN regulates F-actin network organization and turnover at the cell leading edge. (*A*) Kymograph analysis of actin retrograde flow in MTLn3 cells transfected with GFP empty vector control alone or combined with Myc-tagged CIN^{WT}, control siRNA, or CIN siRNA. White lines highlight F-actin speckle flow rates in the lamellipodium (Lp), lamella (Lm), and convergence zone (CZ). [Time bar (*t*): 2 min; scale bar (*d*): 1 μm.] (*B*) F-actin flow maps computed from quantitative FSM analysis of time-lapse movies of the cells depicted in *A*. Flow rates are color-coded and range from fast flow in red to slow flow in blue. Flow maps have been averaged over six frames (i.e., 30 s) and have been created with the same speed scale to allow comparison of cells under different conditions. (Scale bar: 5 μm.) (*C*) Average F-actin flow rates measured at the leading edge and 2.5 μm from the leading edge of transfected cells (± SEM); $n = 16$–20 cells for each condition. The experiment was repeated at least four times. *$P < 0.0001$ compared with GFP-expressing cells. (*D*) Average width of the lamellipodium (± SEM) determined from kymographs of FSM movies of cells transfected with control or CIN siRNA; $n \geq 20$ cells for each condition, with a minimum of 25 measurements per cell. Ctrl, control. *$P < 0.0001$ compared with control siRNA.

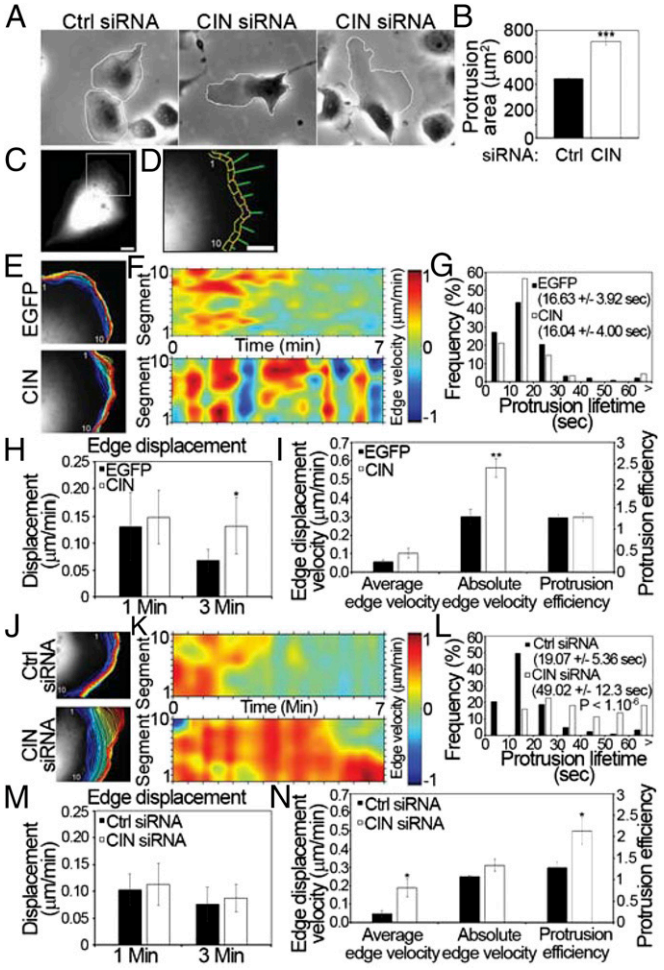

Fig. 9. Leading edge dynamics are regulated by CIN. (*A*) Phase-contrast images of control siRNA and CIN siRNA cells (Movies S5 and S6). (*B*) Average protrusion area (± SEM) measured in control siRNA (n = 122 cells) and CIN siRNA (n = 137 cells) cells at 3 min after EGF stimulation. ***$P < 0.0001$ compared with control siRNA cells. (*C*) Example of GFP-expressing cell. The white box indicates the region of interest for edge analysis. (Scale bar: 10 μm.) (*D*) Sampling windows (numbered 1–10) of 1-μm depth placed at the cell edge and used to quantify cell edge dynamics. Green arrows represent cell edge velocity vectors. (Scale bar: 5 μm.) (*E–N*) MTLn3 cells transfected with (*E*, *Upper*) EGFP empty vector control, (*E*, *Lower*) EGFP + Myc-tagged CIN^{WT}, (*J*, *Upper*) EGFP + control siRNA, or (*J*, *Lower*) EGFP + CIN siRNA were analyzed by time-lapse microscopy during EGF stimulation. Fluorescent images of EGFP were taken every 10 s for 7 min. Leading edge dynamics were analyzed using Matlab, with edge displacement evolution encoded from blue (t = 0 min) to red (t = 7 min). (*F* and *K*) Kymographs of protrusion and retraction dynamics of the leading edge of MTLn3 cells. Edge displacements are encoded with warm color (red) for protrusion and cold color (blue) for retraction. (*G* and *L*) Frequency histograms of protrusion lifetime in (*G*) EGFP (black) or EGFP + CIN^{WT} (white) cells or (*L*) EGFP + control siRNA (black) or EGFP + CIN siRNA (white) cells during 7 min after EGF stimulation quantified from the edge analysis in Matlab. The numbers in the top right indicate the average protrusion lifetime (± SEM) for each condition. ***$P < 1.10^{-6}$ compared with control siRNA cells. (*H* and *M*) Average leading edge displacement (± SEM) obtained from the protrusion analysis in Matlab at 1 and 3 min after EGF stimulation. *$P < 0.05$ compared with control EGFP cells. (*I* and *N*) Analysis of overall edge displacement during EGF stimulation: average edge velocity (± SEM), absolute edge velocity (± SEM), and protrusion efficiency (± SEM) of a 10-μm leading edge section of MTLn3 cells. The graphs depict measurement of four independent experiments, with an average of 15–25 cells in each condition. Ctrl, control. *$P < 0.05$ vs. control siRNA cells; **$P < 0.01$ compared with control EGFP cells.

Interestingly, CIN depletion (Fig. 8 and Movie S4) did not significantly affect F-actin flow rates in either the lamellipodium (1.701 ± 0.090 μm/min) or the lamella (0.565 ± 0.034 μm/min) compared with cells treated with control siRNA (1.538 ± 0.066 μm/min in the lamellipodium and 0.562 ± 0.014 μm/min in the lamella) (Fig. 8*C* and Movie S3). However, CIN knockdown induced a widening of the lamellipodium (1.259 ± 0.062 μm compared with 0.819 ± 0.070 μm in control siRNA cells) (Fig. 8 *A* and *D*), suggesting a stabilization of the filaments at the leading edge.

Quantitative FSM analysis of F-actin retrograde flow was used to obtain spatial maps of F-actin flow speed (Fig. 8*B*). These maps confirmed the results obtained with kymograph analysis but additionally, revealed changes in flow speeds characterizing the lamellipodium/lamella transition (from fast flow in red to slow flow in blue in Fig. 8*B*) continuously across the breadth of the protrusion. Compared with control cells, cells expressing CIN displayed a wider region of rapid actin retrograde flow (Fig. 8*B*). No significant difference was observed in CIN-depleted cells compared with control cells. Taken together, these results indicate that CIN expression increases F-actin retrograde flow and affects the lamellipodium/lamella distribution in the protrusion. This phenotype was previously described in cells with enhanced cofilin activity (51), thus confirming the role of CIN in activating cofilin at the cell leading edge.

CIN Depletion Affects Cell Edge Morphology upon EGF Stimulation. Having shown the recruitment and activity of CIN at the cell edge during EGF stimulation and knowing that cofilin activation and actin polymerization are required for the generation of protrusive force in migrating cells, we next investigated the effects of CIN on leading edge protrusion dynamics. We first observed the effect of endogenous CIN depletion on the cell edge response to EGF stimulation (Fig. 9*A*). Control MTLn3 cells exhibited a compact cell shape associated with the infrequent extension of small, short-lived protrusions (Movie S5). On exposure to EGF, the cells rapidly responded by initiating protrusion and extending a broad, uniform lamella around much of the cell perimeter (Movie S5). In marked contrast, CIN-depleted cells in the unstimulated state exhibited extensive long-lived protrusions and were highly motile, often moving in a straight direction for extended periods of time (Movie S6). Addition of EGF had little effect on the morphology or behavior of the cells (Movie S6), suggesting that CIN is required for the cells to sense EGF; 85% of the cells exhibited very large, extended protrusions, with a significant protrusion average area of 718.6 ± 27.3 μm^2 in CIN siRNA cells compared with 441.1 ± 6.2 μm^2 in control cells (Fig. 9*B*). In addition, 50% of the cells also generated two or more protrusions at random points around the cell periphery (Fig. 9*A* and Movie S6). This phenotype is remarkably similar to that observed by overall knockdown of cofilin expression in MTLn3 cells (11) and consistent with the increase of inactive (phosphorylated) endogenous cofilin observed in these cells (Fig. 3).

CIN Activity Coordinates the Cell Edge Protrusion and Retraction During EGF Stimulation. We next investigated in more detail the role of CIN on leading edge protrusion dynamics (Fig. 9 *C–N*). In control cells, protrusion events along the cell edge propagated upon EGF stimulation for about 3–4 min (visible in kymographs as red regions in Fig. 9*F*, *Upper*), and then, mainly retraction events took place (visible in kymographs as blue regions in Fig. 9*F*, *Upper*). In cells expressing CIN^{WT}, EGF addition induced high-velocity protrusions of the cell edge that alternated with high-velocity retraction events (visible in kymographs as red and blue bands, respectively, in Fig. 9*F*, *Lower*). These data suggest that CIN regulates the spatiotemporal coordination of leading edge movements. To examine how CIN affected the productive edge advancement during EGF stimulation, we calculated the protrusion parameters (Fig. 9 *G–I*). We found that CIN-expressing cells had a comparable protrusion lifetime to control cells (Fig. 9*G*). The displacement of the cell leading edge at 1 min after EGF addition was similar in control cells and cells overexpressing CIN (Fig. 9*H*). Interestingly, we observed a significant increase in the protrusion at 3 min in cells overexpressing CIN

compared with control cells (Fig. 9*H*). These results correlate with the effects of CIN on the actin free barbed end formation that we observed in Fig. 7. We next analyzed the protrusion dynamics of the cells expressing empty vector control or Myc-CIN^{WT} during the overall EGF stimulation (i.e., 7 min). Analysis of the average edge displacement velocity, which is a measure of net edge advancement, revealed no significant difference between control cells and CIN^{WT}-expressing cells ($P = 0.17$) (Fig. 9*I*). However, the average absolute edge displacement speed of cells overexpressing CIN was significantly higher compared with control cells, indicating that even low levels of additional CIN accelerate the instantaneous movement of the leading edge. To analyze the effect of CIN on the productive advancement of the cell, we next calculated the protrusion efficiency as the ratio between the distances that the edge traveled in the protruding and the retracting states (Fig. 9*I*). Thus, a ratio equal to one indicates that protrusion and retraction events equal one another, resulting in retention of a constant average position of the cell edge. Conversely, a ratio greater than one indicates a net advancement of the entire leading edge. The protrusion efficiency scores of control and CIN-overexpressing cells were both statistically greater than one, indicating that cells significantly protrude on average. However, despite higher instantaneous edge displacement velocities of cells overexpressing CIN compared with control cells, no significant difference was measured between both conditions ($P = 0.95$). These results indicate that, by enhancing both protruding and retracting state velocities, cells overexpressing CIN maintain a protrusion efficiency identical to control cells.

We next analyzed leading edge dynamics of CIN-depleted cells upon EGF stimulation (Fig. 9*J*). The kymographs shown in Fig. 9*K* revealed that, in nontargeting siRNA oligo cells, the protrusion events occurred right after EGF addition for about 3 min (red regions in Fig. 9*K*), and then, the retraction events took place (blue regions in Fig. 9*K*). Interestingly, we continuously observed protrusion events in CIN-ablated cells, confirming the observation made in Fig. 9*A*. Quantification of protrusion lifetime showed an increase of cells that protrude for 30 s or more in the absence of CIN (61.4% of cells) compared with control cells (11.4% of cells) (Fig. 9*L*). The displacement of the cell leading edge at 1 and 3 min was similar in control and CIN-depleted cells (Fig. 9*M*). However, the analysis of the average edge displacement velocity revealed a significantly higher net velocity in cells depleted in CIN compared with control cells. In contrast, the instantaneous edge velocity was similar in both cases ($P = 0.094$), thus indicating that CIN-depleted cells spent most of their time in a protruding state (Fig. 9 *J* and *N*). As a result, the protrusion efficiency was much higher in these cells than in control cells (Fig. 9*N*). These data suggest that depletion of CIN induces a loss of the balance between protrusion and retraction events along the cell edge during EGF stimulation, favoring the protrusion events.

Altogether, these data indicate that CIN regulates the temporal coordination of the leading edge, likely by affecting cofilin activity levels.

Discussion

Tumor cell invasion during metastasis is enhanced by orientation of cancer cells toward blood vessels and the surrounding environments. Directed cell migration—or chemotaxis—results from the sensing of an extracellular cue. This event processes through complex signaling networks and the production of a coordinated response to organize the cytoskeletal machinery. Signals that promote cell motility are often correlated with increased cofilin activity, whereas those inhibiting motility enhance cofilin phosphorylation (2, 8). In breast cancer cells, EGF-stimulated chemotaxis is used as a mechanism to induce the first step of cell orientation: the lamellipodia extension. This process relies on the tight regulation of cofilin activity to induce two transients of actin polymerization. Although the mechanisms of cofilin activation during the first transient have been well-characterized (11, 22, 34, 42, 52, 53), the formation of the second transient, which requires both cofilin and PI3-kinase activities and leads to full protrusion of the leading edge membrane, remains unclear. We show here that the CIN is an important component of a PI3-kinase–mediated, Rac1-dependent signaling mechanism that activates cofilin downstream of EGF receptor stimulation in MTLn3 mammary carcinoma cells. CIN is induced to translocate from a predominantly cytosolic location to regions at the cell edge where actin polymerization and lamellipodium protrusion are occurring (Fig. 1). This translocation of CIN begins as early as 1 min and reaches its maximum at 3 min, correlating with a decrease in inactive P-cofilin at the cell edge (Fig. 2) and a peak of actin filament free barbed end formation (Fig. 7). Moreover, depletion of endogenous CIN using siRNA antagonized cofilin activation at the cell periphery induced by EGF, instead causing P-cofilin levels to increase (Fig. 3). These data strongly suggest that CIN is a component of the EGF-stimulated cofilin regulatory mechanism that controls MTLn3 cell leading edge actin dynamics.

Spatial activation of cofilin is critical to cell movement; photoactivation of caged cofilin at specific regions within the cell can initiate membrane protrusion (10). Thus, localized regulation of cofilin activators, such as CIN and SSH, might be a critical factor in cofilin cell protrusion. Recent studies have shown that compartmentalization of CIN and cofilin in protease-activated receptor2-mediated chemotaxis requires the scaffold ARB proteins to initiate membrane extension. Interestingly, in EGF-stimulated cells, our study showed that β-arrestins had no effect on CIN translocation to the leading edge. Instead, it requires PI3-kinase/Rac activity (Fig. 4), and importantly, it is dependent on cofilin expression, because cofilin depletion abrogates CIN accumulation at the cell edge (Fig. 6). Interestingly, whereas SSH has been reported to accumulate at the membrane protrusion in response to SDF-1α stimulation in Jurkat cells (54), our data showed that, in contrast to CIN, SSH does not seem to be involved in EGF action in MTLn3 cells. Indeed, we found that (*i*) SSH-1L does not translocate from the cytosol to the cell leading edge after EGF addition and that (*ii*) SSH-1L is primarily associated with actin stress fibers but not the leading edge in MTLn3 cells. A distinct localization pattern between CIN and SSH has been also reported in HeLa cells during cell division. Moreover, the two phosphatases are not functionally redundant in the context of mitosis, because siRNA-mediated depletion of either protein in the same cell type caused distinct temporal changes in P-cofilin levels in synchronized mitotic cells (29, 55). Therefore, based on studies by other groups and our work, we conclude that CIN and SSH might differ in their mode of activation, subcellular distribution, and regulatory function. Each phosphatase may activate cofilin in specific functional contexts. Our data indicate that CIN fits the criteria as a primary regulator of the second peak of MTLn3 cell actin polymerization in response to EGF stimulation.

We observed that expression of CIN enhanced F-actin retrograde flow throughout large parts of the protrusion (Fig. 8), a finding consistent with other studies that showed an increase in actin retrograde flow downstream of cofilin activation (51, 56, 57). Decrease of endogenous CIN by siRNA did not reduce retrograde flow, which one could have expected with lower levels of active cofilin. However, it did induce a significant widening of the lamellipodium (Fig. 8). A similar increase in lamellipodial F-actin has been recently described after instantaneous inactivation of cofilin (5). These data suggest that CIN depletion enhanced P-cofilin levels that led to a decrease in filament disassembly. Together, our data confirm that CIN regulates cofilin-dependent actin turnover.

Overexpression of CIN caused the cells to have faster rates of both protrusion and retraction, resulting in only a small net edge protrusion. Cells displayed a similar migration velocity compared with control cells (Fig. S5*A*). These results corroborate and extend the observations by Delorme et al. (51) in Ptk1 cells, where

an increase of cofilin activity downstream of active Rac1 was associated with reduced net edge advancement. This result was shown to be caused by the need for an optimal level of cofilin activity to maintain the coupling between the lamellipodium and the lamella actin networks to promote effective protrusion. We propose that, in MTLn3 cells stimulated with EGF, CIN is important to maintain the phosphocycling of a pool of cofilin that is being phosphorylated and inactivated by the action of EGF-activated LIMK1 (45). When CIN is present and active, F-actin turnover is promoted by local activation of cofilin, maintaining the balance between protrusion and retraction that enables the cell to rapidly respond to growth factor stimulus. It is of interest that depletion of CIN activity is associated with an increased rate of cell edge protrusion, resulting in greater net protrusion. This result differs from EGF-stimulated MTLn3 cells depleted in cofilin, in which both F-actin accumulation at the cell edge and protrusion rate are decreased (12). Active cofilin is critical for the initiation of the protrusion at 1 min upon EGF stimulation, and we have now shown in this study that CIN is required to regulate cofilin activity at the cell edge to generate persistent membrane protrusion at 3 min after addition of EGF. Therefore, in CIN-depleted cells, the first pool of active cofilin, which depends on PLCγ activity but not on dephosphorylation mechanisms, is available to initiate the protrusion. Then, during the course of EGF stimulation, LIMK1 activity predominates, inactivating cofilin, decreasing the depolymerization of F-actin, and subsequently, reducing the amount of diffusible actin in cytoplasm (6), thereby preventing a rapid F-actin treadmilling. However, the lamellipodial protrusion still slowly extended (Fig. 9), suggesting the presence of a small pool of G-actin monomers available from other sources than cofilin (6). Because CIN-depleted cells have a higher protrusion efficiency compared with control cells, one would expect an increase in cell migration velocity. However, no difference was detected (Fig. S5*A*). These data may result from the absence of a cofilin activation/inactivation cycle at the leading edge of CIN-depleted cells during EGF stimulation. Because the motility cycle requires not only protrusion of the cell edge but also, formation of adhesion and cell body translocation, our results could indicate that CIN controls other steps than protrusion during cell migration. We have observed that CIN-depleted cells are more adherent compared with control siRNA cells, suggesting that CIN may affect the focal adhesion turnover, leading to a defect in cell body displacement and/or rear detachment (Fig. S5 *B* and *C*), which in turn, might affect cell velocity. Altogether, our findings support a direct role of CIN in cofilin-mediated leading edge protrusion during stimulated cell migration.

The localized, coordinated regulation of cofilin phosphocycling is an important mechanism for modulating cell morphology, cytoskeletal dynamics, and behavior (30). Mammalian cells have evolved multiple cofilin regulatory mechanisms, and it is likely that distinct upstream signals in different cells may selectively activate specific pathways to enact various cofilin-dependent functions. CIN has been established biochemically to be a dedicated cofilin/ADF (actin depolymerizing factor) phosphatase (29). Our findings place CIN in an EGF-initiated signaling pathway involving PI3-kinase, Rac1 activity and cofilin. In this study, we extend the roles of CIN to the growth factor-dependent regulation of leading edge actin dynamics in MTLn3 carcinoma cells. It will be of interest in future studies to investigate the role(s) of CIN in cancer cell invasion and metastasis.

Materials and Methods

Immunofluorescence Microscopy. For microscopic observations, MTLn3 (obtained from J. Condeelis, Albert Einstein College of Medicine, Bronx, NY) cells were plated in six-well plates containing glass coverslips coated with collagen at 24 μg/mL in MEM containing 4% (vol/vol) FBS and transfected as described above. To determine the localization of overexpressed CIN during EGF stimulation, cells were cotransfected with GFP empty vector control (50 ng per well) and Myc-tagged CIN (200 ng per well) for 6 h; MTLn3 cells were then starved for 3 h in serum-free medium and stimulated with EGF at a final concentration of 5 nM for the period indicated. Cells were then fixed for 20 min with 4% formaldehyde converted from paraformaldehyde, permeabilized in 0.5% Triton X-100 for 10 min, and blocked with 3% (wt/vol) BSA in PBS for 1 h. The cells were then incubated with primary antibodies for 1 h, washed three times for 5 min each with PBS, and then, stained with secondary antibodies for another 1 h. For visualization of F-actin, cells were labeled with Alexa-phalloidin for 30 min. Cells were mounted on glass slides in medium containing antifade reagents (Prolong Gold; Molecular Probes). For P-cofilin and cofilin immunostaining, cells were fixed in 4% formaldehyde for 20 min, permeabilized with −20 °C methanol for 3 min, and blocked in 2% goat serum/1% BSA in Tris-buffered saline for 1 h before immunostaining. After blocking and immunostaining, coverslips were mounted on glass slides with Prolong Antifade. Epifluorescence images of fixed cells were acquired on an inverted microscope (Eclipse TE 2000-U; Nikon) equipped with an electronically controlled shutter, filter wheels, and a 14-bit cooled CCD (charge couple device) camera (Cool SNAP HQ; Photometrics) controlled by MetaMorph software (Universal Imaging Corp.) by using a 60×/1.4 N.A. Plan Apo DIC Objective Lens (Nikon).

Immunofluorescence Analysis. Imaging was performed on healthy cells only (i.e., well-spread). All cells were scored blindly for each category. Fluorescence intensity of F-actin, CIN, SSH, GFP, free barbed ends, P-cofilin, or cofilin measured from the cell edge to the cell center was quantified on cell protrusions free of cell/cell contact using custom software written in Matlab (Mathworks). Bands of constant distance to the cell edge were constructed, and individual fluorescence intensities were accumulated and averaged in each band to produce fluorescence intensities vs. distance to cell edge graphs. The data shown represent one experiment and are averaged for between 15 and 20 cells for each independent experiment. The exact number of cells analyzed for each experiment is indicated. Representative quantification from at least three experiments is shown.

Barbed End Assay. To measure the number of free barbed ends in response to EGF and stain for F-actin with Rhodamine-phalloidin, we used a previously described assay (34).

F-Actin Cosedimentation Assays. F-actin cosedimentation assays were performed using the Actin Binding Protein Spin Down Assay Biochem Kit as described by the manufacturer (BK013; Cytoskeleton, Inc.). Briefly, 2 μM BSA, α-actinin, or CIN was incubated with 40 μL freshly polymerized nonmuscle actin (F-actin; 21 μM) or 40 μL F-actin polymerization buffer as control (10 mM Tris·Cl, pH 7.5, 50 mM KCl, 2 mM $MgCl_2$, 1 mM ATP) in a 50 μL final volume for 30 min at 24 °C. After incubation, the protein plus F-actin solutions were subjected to centrifugation (150,000 × *g* for 1.5 h at 24 °C). Supernatants were carefully removed, and pellets were resuspended in 50 μL distilled water. Equal amounts of pellet and supernatant fractions (20 μL) were submitted to SDS/PAGE and analyzed by Coomassie Blue staining and immunoblotting as indicated. Purified His-CIN protein was purified from *Escherichia coli* as described previously (29) and in *SI Materials and Methods*. For GFP-CIN, the protein was expressed from HeLa cells, immunoprecipitated using GFP-Trap (Chromotek), and eluted with 200 mM glycine.

FSM. MTLn3 cells transfected with GFP (9 h), GFP and Myc-CIN WT (9 h), control siRNA (96 h), or CIN siRNA (96 h) as described in *SI Materials and Methods* were plated on coverslips coated with collagen. Cells were prepared for live-cell microscopy as described (58). Actin FSM time-lapse series were acquired at 5-s intervals for 10 min by using a 100×/1.4 N.A. Plan Apo Objective Lens (Nikon) on the spinning disk confocal microscope system described in ref. 59 with either a 14-bit Orca II or a CoolSnapHQ Camera.

FSM Analysis and Quantification. F-actin flow rates at the cell leading edge were measured by kymograph analysis as described (60). At least five randomly placed lines normal to the cell edge were used to construct five kymographs of each cell, and five flow rate measures were calculated for each region (lamellipodium/lamella) in each kymograph. FSM time-lapse image series were analyzed using the *fsmCenter* software package written in Matlab (Mathworks) (61).

Leading Edge Dynamics. MTLn3 cells expressing Myc-tagged CIN^{WT} or CIN-depleted cells were plated on glass coverslips coated with collagen, starved for 3 h, and mounted in chambers for live-cell microscopy. For cell protrusion measurements, cells were cotransfected with GFP empty vector to follow the edge of the cells. Movies were analyzed using the *fsmCenter* package written in Matlab (62).

Statistical analysis was performed using a two-tailed Student's *t* test.

ACKNOWLEDGMENTS. We thank J. Bamburg for antibodies mAb22 (mouse cofilin antibody) and 4321 (rabbit P-cofilin antibody) and critically reading the manuscript. We also thank T. Huang for shRNA constructs. This work was supported by National Institutes of Health Grant GM44428 (to C.D.) and American Heart Association Western States Affiliate Grant 0765049Y (to C.D.). This is Manuscript 28039 from The Scripps Research Institute.

1. Pollard TD, Borisy GG (2003) Cellular motility driven by assembly and disassembly of actin filaments. *Cell* 112(4):453–465.
2. DesMarais V, Ghosh M, Eddy R, Condeelis J (2005) Cofilin takes the lead. *J Cell Sci* 118(Pt 1):19–26.
3. Pollard TD, Blanchoin L, Mullins RD (2000) Molecular mechanisms controlling actin filament dynamics in nonmuscle cells. *Annu Rev Biophys Biomol Struct* 29:545–576.
4. Hotulainen P, Paunola E, Vartiainen MK, Lappalainen P (2005) Actin-depolymerizing factor and cofilin-1 play overlapping roles in promoting rapid F-actin depolymerization in mammalian nonmuscle cells. *Mol Biol Cell* 16(2):649–664.
5. Vitriol EA, Wise AL, Berginski ME, Bamburg JR, Zheng JQ (2013) Instantaneous inactivation of cofilin reveals its function of F-actin disassembly in lamellipodia. *Mol Biol Cell* 24(14):2238–2247.
6. Kiuchi T, Ohashi K, Kurita S, Mizuno K (2007) Cofilin promotes stimulus-induced lamellipodium formation by generating an abundant supply of actin monomers. *J Cell Biol* 177(3):465–476.
7. Ono S (2007) Mechanism of depolymerization and severing of actin filaments and its significance in cytoskeletal dynamics. *Int Rev Cytol* 258:1–82.
8. Bamburg JR (1999) Proteins of the ADF/cofilin family: Essential regulators of actin dynamics. *Annu Rev Cell Dev Biol* 15:185–230.
9. Gungabissoon RA, Bamburg JR (2003) Regulation of growth cone actin dynamics by ADF/cofilin. *J Histochem Cytochem* 51(4):411–420.
10. Ghosh M, et al. (2004) Cofilin promotes actin polymerization and defines the direction of cell motility. *Science* 304(5671):743–746.
11. Mouneimne G, et al. (2006) Spatial and temporal control of cofilin activity is required for directional sensing during chemotaxis. *Curr Biol* 16(22):2193–2205.
12. Sidani M, et al. (2007) Cofilin determines the migration behavior and turning frequency of metastatic cancer cells. *J Cell Biol* 179(4):777–791.
13. Tahtamouni LH, Shaw AE, Hasan MH, Yasin SR, Bamburg JR (2013) Non-overlapping activities of ADF and cofilin-1 during the migration of metastatic breast tumor cells. *BMC Cell Biol* 14:45.
14. Bravo-Cordero JJ, Magalhaes MA, Eddy RJ, Hodgson L, Condeelis J (2013) Functions of cofilin in cell locomotion and invasion. *Nat Rev Mol Cell Biol* 14(7):405–415.
15. Wang W, Eddy R, Condeelis J (2007) The cofilin pathway in breast cancer invasion and metastasis. *Nat Rev Cancer* 7(6):429–440.
16. Wang W, et al. (2006) The activity status of cofilin is directly related to invasion, intravasation, and metastasis of mammary tumors. *J Cell Biol* 173(3):395–404.
17. Wang W, et al. (2004) Identification and testing of a gene expression signature of invasive carcinoma cells within primary mammary tumors. *Cancer Res* 64(23):8585–8594.
18. van Rheenen J, Condeelis J, Glogauer M (2009) A common cofilin activity cycle in invasive tumor cells and inflammatory cells. *J Cell Sci* 122(Pt 3):305–311.
19. Bamburg JR, et al. (2010) ADF/Cofilin-actin rods in neurodegenerative diseases. *Curr Alzheimer Res* 7(3):241–250.
20. Gorbatyuk VY, et al. (2006) Mapping the phosphoinositide-binding site on chick cofilin explains how PIP2 regulates the cofilin-actin interaction. *Mol Cell* 24(4):511–522.
21. Yonezawa N, Nishida E, Iida K, Yahara I, Sakai H (1990) Inhibition of the interactions of cofilin, destrin, and deoxyribonuclease I with actin by phosphoinositides. *J Biol Chem* 265(15):8382–8386.
22. van Rheenen J, et al. (2007) EGF-induced PIP2 hydrolysis releases and activates cofilin locally in carcinoma cells. *J Cell Biol* 179(6):1247–1259.
23. Bernstein BW, et al. (2000) Intracellular pH modulation of ADF/cofilin proteins. *Cell Motil Cytoskeleton* 47(4):319–336.
24. Frantz C, et al. (2008) Cofilin is a pH sensor for actin free barbed end formation: Role of phosphoinositide binding. *J Cell Biol* 183(5):865–879.
25. Arber S, et al. (1998) Regulation of actin dynamics through phosphorylation of cofilin by LIM-kinase. *Nature* 393(6687):805–809.
26. Toshima J, et al. (2001) Cofilin phosphorylation by protein kinase testicular protein kinase 1 and its role in integrin-mediated actin reorganization and focal adhesion formation. *Mol Biol Cell* 12(4):1131–1145.
27. Yang N, et al. (1998) Cofilin phosphorylation by LIM-kinase 1 and its role in Rac-mediated actin reorganization. *Nature* 393(6687):809–812.
28. Niwa R, Nagata-Ohashi K, Takeichi M, Mizuno K, Uemura T (2002) Control of actin reorganization by Slingshot, a family of phosphatases that dephosphorylate ADF/cofilin. *Cell* 108(2):233–246.
29. Gohla A, Birkenfeld J, Bokoch GM (2005) Chronophin, a novel HAD-type serine protein phosphatase, regulates cofilin-dependent actin dynamics. *Nat Cell Biol* 7(1):21–29.
30. Huang TY, DerMardirossian C, Bokoch GM (2006) Cofilin phosphatases and regulation of actin dynamics. *Curr Opin Cell Biol* 18(1):26–31.
31. Soosairajah J, et al. (2005) Interplay between components of a novel LIM kinase-slingshot phosphatase complex regulates cofilin. *EMBO J* 24(3):473–486.
32. Cai L, Marshall TW, Uetrecht AC, Schafer DA, Bear JE (2007) Coronin 1B coordinates Arp2/3 complex and cofilin activities at the leading edge. *Cell* 128(5):915–929.
33. Kestler C, et al. (2014) Chronophin dimerization is required for proper positioning of its substrate specificity loop. *J Biol Chem* 289(5):3094–3103.
34. Mouneimne G, et al. (2004) Phospholipase C and cofilin are required for carcinoma cell directionality in response to EGF stimulation. *J Cell Biol* 166(5):697–708.
35. Huang TY, Minamide LS, Bamburg JR, Bokoch GM (2008) Chronophin mediates an ATP-sensing mechanism for cofilin dephosphorylation and neuronal cofilin-actin rod formation. *Dev Cell* 15(5):691–703.
36. Sun CX, Magalhães MA, Glogauer M (2007) Rac1 and Rac2 differentially regulate actin free barbed end formation downstream of the fMLP receptor. *J Cell Biol* 179(2):239–245.
37. Zoudilova M, et al. (2010) beta-Arrestins scaffold cofilin with chronophin to direct localized actin filament severing and membrane protrusions downstream of protease-activated receptor-2. *J Biol Chem* 285(19):14318–14329.
38. Condeelis J, Pollard JW (2006) Macrophages: Obligate partners for tumor cell migration, invasion, and metastasis. *Cell* 124(2):263–266.
39. Wyckoff J, et al. (2004) A paracrine loop between tumor cells and macrophages is required for tumor cell migration in mammary tumors. *Cancer Res* 64(19):7022–7029.
40. Chan AY, Bailly M, Zebda N, Segall JE, Condeelis JS (2000) Role of cofilin in epidermal growth factor-stimulated actin polymerization and lamellipod protrusion. *J Cell Biol* 148(3):531–542.
41. Chan AY, et al. (1998) EGF stimulates an increase in actin nucleation and filament number at the leading edge of the lamellipod in mammary adenocarcinoma cells. *J Cell Sci* 111(Pt 2):199–211.
42. Song X, et al. (2006) Initiation of cofilin activity in response to EGF is uncoupled from cofilin phosphorylation and dephosphorylation in carcinoma cells. *J Cell Sci* 119(Pt 14):2871–2881.
43. Chen L, et al. (2003) Two phases of actin polymerization display different dependencies on PI(3,4,5)P3 accumulation and have unique roles during chemotaxis. *Mol Biol Cell* 14(12):5028–5037.
44. Hill K, et al. (2000) Specific requirement for the p85-p110alpha phosphatidylinositol 3-kinase during epidermal growth factor-stimulated actin nucleation in breast cancer cells. *J Biol Chem* 275(6):3741–3744.
45. Zebda N, et al. (2000) Phosphorylation of ADF/cofilin abolishes EGF-induced actin nucleation at the leading edge and subsequent lamellipod extension. *J Cell Biol* 151(5):1119–1128.
46. Kölsch V, Charest PG, Firtel RA (2008) The regulation of cell motility and chemotaxis by phospholipid signaling. *J Cell Sci* 121(Pt 5):551–559.
47. Welch HC, Coadwell WJ, Stephens LR, Hawkins PT (2003) Phosphoinositide 3-kinase-dependent activation of Rac. *FEBS Lett* 546(1):93–97.
48. El-Sibai M, et al. (2007) Cdc42 is required for EGF-stimulated protrusion and motility in MTLn3 carcinoma cells. *J Cell Sci* 120(Pt 19):3465–3474.
49. Simard E, et al. (2013) β-Arrestin regulation of myosin light chain phosphorylation promotes AT1aR-mediated cell contraction and migration. *PLoS One* 8(11):e80532.
50. Ma X, Zhao Y, Daaka Y, Nie Z (2012) Acute activation of β2-adrenergic receptor regulates focal adhesions through βArrestin2- and p115RhoGEF protein-mediated activation of RhoA. *J Biol Chem* 287(23):18925–18936.
51. Delorme V, et al. (2007) Cofilin activity downstream of Pak1 regulates cell protrusion efficiency by organizing lamellipodium and lamella actin networks. *Dev Cell* 13(5):646–662.
52. Leyman S, et al. (2009) Unbalancing the phosphatidylinositol-4,5-bisphosphate-cofilin interaction impairs cell steering. *Mol Biol Cell* 20(21):4509–4523.
53. Tania N, Prosk E, Condeelis J, Edelstein-Keshet L (2011) A temporal model of cofilin regulation and the early peak of actin barbed ends in invasive tumor cells. *Biophys J* 100(8):1883–1892.
54. Nishita M, et al. (2005) Spatial and temporal regulation of cofilin activity by LIM kinase and Slingshot is critical for directional cell migration. *J Cell Biol* 171(2):349–359.
55. Kaji N, et al. (2003) Cell cycle-associated changes in Slingshot phosphatase activity and roles in cytokinesis in animal cells. *J Biol Chem* 278(35):33450–33455.
56. Flynn KC, et al. (2012) ADF/cofilin-mediated actin retrograde flow directs neurite formation in the developing brain. *Neuron* 76(6):1091–1107.
57. Zhang XF, Hyland C, Van Goor D, Forscher P (2012) Calcineurin-dependent cofilin activation and increased retrograde actin flow drive 5-HT-dependent neurite outgrowth in Aplysia bag cell neurons. *Mol Biol Cell* 23(24):4833–4848.
58. Gupton SL, et al. (2005) Cell migration without a lamellipodium: Translation of actin dynamics into cell movement mediated by tropomyosin. *J Cell Biol* 168(4):619–631.
59. Adams MC, et al. (2003) A high-speed multispectral spinning-disk confocal microscope system for fluorescent speckle microscopy of living cells. *Methods* 29(1):29–41.
60. Salmon WC, Adams MC, Waterman-Storer CM (2002) Dual-wavelength fluorescent speckle microscopy reveals coupling of microtubule and actin movements in migrating cells. *J Cell Biol* 158(1):31–37.
61. Danuser G, Waterman-Storer CM (2006) Quantitative fluorescent speckle microscopy of cytoskeleton dynamics. *Annu Rev Biophys Biomol Struct* 35:361–387.
62. Machacek M, Danuser G (2006) Morphodynamic profiling of protrusion phenotypes. *Biophys J* 90(4):1439–1452.